Bianisotropy and magnetism in plasmonic gratings

Matthias Kraft,[*,†,¶] Avi Braun,[*,†,¶] Yu Luo,[‡] Stefan A. Maier,[†] and John B. Pendry[†]

Blackett Laboratory, Department of Physics, Imperial College London, London SW7 2AZ, United Kingdom, and School of Electrical and Electronic Engineering, Nanyang Technological University, Nanyang Avenue 639798, Singapore

E-mail: matthias.kraft09@imperial.ac.uk; a.braun@imperial.ac.uk

Abstract

We present a simple design to achieve bianisotropy at visible wavelengths: an ultrathin plasmonic grating made of a gold grating covered by a thin flat layer of gold. We show experimentally and through simulations that the grating exhibits magnetoelectric coupling and features asymmetric reflection and absorption, all that with a device thickness of a tenth of the operating wavelength. We compared the spectral results and retrieved the effective material parameters of different polarizations and devices. We show that both asymmetry and strong coupling between the incoming light and the optically interacting surfaces are required for obtaining asymmetric optical behavior in metasurfaces.

[*]To whom correspondence should be addressed
[†]Imperial College London
[‡]Nanyang Technological University
[¶]These authors contributed equally

Keywords

Bianisotropy, Magnetism, Plasmonics, Grating, Metamaterial

In their seminal book,[1] Landau and Lifshitz commented on the insignificance of magnetism at optical frequencies. Yet, several recent studies have shown that magnetic effects are present in optical systems[2–4] particularly those containing metals that have been structured in some way. The mechanism is familiar from the concept of metamaterials whereby novel electrical and magnetic properties can be found by engineering the microstructure.[5–8] Here we present an experimental study of a structured system, in our case a grating, and interpret the data in terms of effective parameters of an equivalent ultrathin layer of metamaterial. Features such as asymmetric reflection will emerge from the interplay of magnetic and electric fields.

Lately, a lot of attention has been given to the development of metasurfaces – textured surfaces at a sub-wavelength scale with tailored electro-magnetic properties.[9–14] These devices are the two-dimensional counterpart of metamaterials and benefit from the advantages of reduced profile, reduced ohmic and magnetic losses, and simpler fabrication processes, thus enabling a range of applications from analogue computing,[15] to 'flat optics'[16] and light harvesting applications,[17,18] to name a few.

A special class of metasurfaces comprises bianisotropic ones, that is, materials exhibiting coupling between the electric and magnetic fields,[19–22] which are described by the constitutive relations:[19] $\mathbf{D} = \boldsymbol{\epsilon}\mathbf{E} + \boldsymbol{\xi}\mathbf{H}$ and $\mathbf{B} = \boldsymbol{\mu}\mathbf{H} + \boldsymbol{\zeta}\mathbf{E}$ (see methods), with the coupling parameters $\boldsymbol{\xi}$ and $\boldsymbol{\zeta}$ relating the displacement current (D) with the magnetic field (H), and the magnetic flux density (B) with the electrical field (E), respectively. A typical characteristic of bianisotropic structures is their asymmetric response depending on which side of the structure they are being probed from.[23]

There is a large body of literature, discussing bianisotropy in the THz[21,24] and GHz regimes,[25–28] with applications in polarization changers,[27,29] asymmetric absorbers/reflectors[25,28] and perfect absorbers.[30] However, in the spectral optical regime, very few experimental studies exists.[29,31,32] Recently, an asymmetric absorber operating in the visible frequency range has been designed,[32] where the asymmetry originates from a dielectric-metal stack of thin Ag nano-holes array patterned over a Silicon-Nitride membrane.

In this paper we show experimentally that asymmetric reflection based on bianisotropy and magneto-electric coupling can be achieved at visible wavelengths simply, using all-metal plasmonic gratings with reduced thickness of the active region, in a design that requires simple and commonly used fabrication methods. Electrodynamic simulations are compared with experimental results and are interpreted in terms of the effective material parameters of the system, which clearly indicate magneto-electric coupling.

Results and discussion

Our bianisotropic metamaterial structure is made of metallic grating lines of width 100nm and a thin conducting layer covering the grating lines and the spacing (also 100nm) between them. These dimensions provide a good tradeoff between entering the sub-wavelength regime, which is necessary for a subsequent metamaterial description and a good uniformity across the grating in the fabrication process. Figure 1 illustrates the bianisotropic structure – 80μm$\times 80\mu$m arrays of a 50nm thick gold grating covered by 10nm layer of gold – next to a 'control' structure with a similar grating array (with slightly larger grating lines due to fabrication imperfections), but lacking the thin gold layer. The two types of gold structures were fabricated by means of electron beam lithography and thermal evaporation on the same quartz substrate. Finally, in order to limit asymmetries in the device only to the active metallic gratings (and not to the substrate, for example) the device was completed by the bonding of another quartz slab on top of the structures (see Methods for fabrication

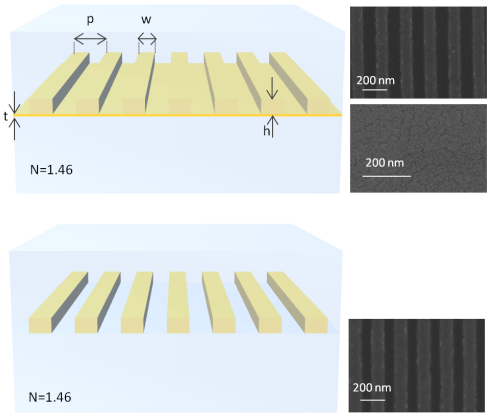

Figure 1: The grating structures. Top: the bianisotropic structure. The letters and arrows indicate the physical dimensions of the structure: w=100nm is the width of grating lines; p=200nm is the grating pitch; t=10 nm is the thickness of the gold layer; and h=55nm is the thickness of the grating lines (including the 10nm gold layer which covers both the grating lines and the spacing between them). Bottom: the control structure with w=110nm; p=200nm, and h=45nm. Both structures are embedded within a medium with n=1.46 at λ=560nm. Placed to the right of the illustrations are zoomed-out and zoomed-in SEM images of the grating structures, taken before the deposition of the thin-film of gold and the attachment of the covering quartz-slide.

details).

Reflection and Transmission spectra

The reflection and transmission spectra of the two types of structures were obtained using a setup of an optical microscope coupled to a grating spectrometer for two linear polarizations: one for which the electric field is aligned with the grating lines ($P = 0$) and one where the polarization is orthogonal to the gratings lines ($P = 90$). For both simulations and measurements the plane wave is normally incident (note that in our experiments, though centered around the normal to the plane of the gratings, the plane wave is distributed throughout the numerical aperture of the objective (N=0.5)). The recording of the transmitted and reflected light was completed via Si photo-diodes coupled to a lock-in amplifier (Figure 2;

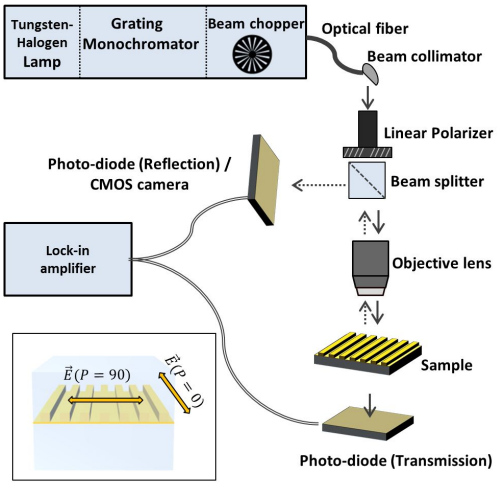

Figure 2: Experimental set-up for transmission and reflection measurements. White light is being diffracted, chopped and coupled to an optical microscope via an optical fiber and beam collimator. The collimated monochromatic light was linearly polarized (along or transversely to the gratings lines) and focused on the structures. A beam-splitter was used to direct the reflected light toward the reflection photo-diode (the path of the reflected light is indicated by dashed arrows), or toward a camera used to assist in locating the structures on the sample. The transmitted/reflected light was recorded on Si photo-diodes connected to a Lock-in amplifier.

see Methods for detailed information about the measurements set-up).

Figure 3 shows the experimental and simulated reflectance spectra for the bianisotropic and the control structures. For polarized light with its electric field *orthogonal* to the grating lines it shows a remarkable difference between the control sample with the metal gratings only, and the bianisotropic sample with the additional thin layer of gold: while the reflection spectra of the control structure (Figure 3c) are inherently indifferent to the direction of incoming light, as expected from an optically symmetric structure, the reflection signal of the gold grating with the additional thin gold layer (Figure 3a) is up to ≈3 times stronger when the device is probed from the side of the thin-film (aka, 'back exposure'), compared to probing from the corrugated side ('front exposure'). For this polarization of the electrical field the bianisotropic and the control devices show a plasmon resonance with maximal reflection at ≈550nm and ≈595nm, respectively – indicating strong coupling to the incident

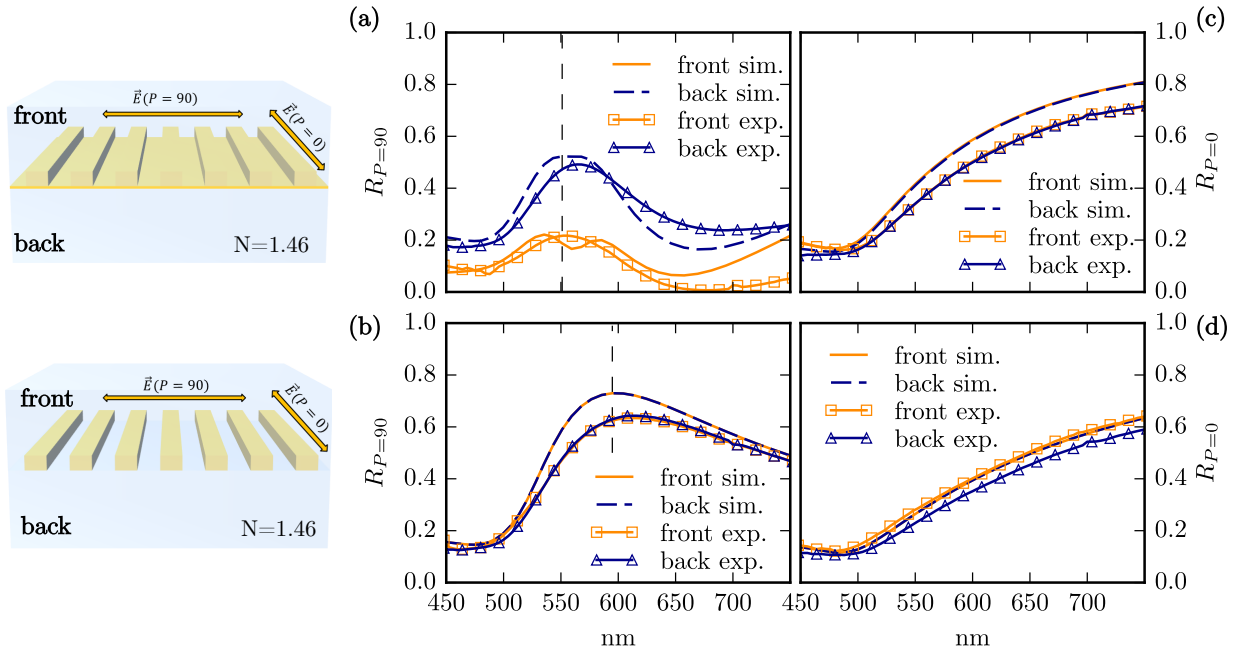

Figure 3: Reflectance spectra. Open triangles and squares are the experimental results for 'back' and 'front' exposure, as defined in the illustration on the left to the plots; blue dashed and orange solid lines correspond to numerical simulations of 'back' and 'front' exposures. a) bianisotropic structure probed with orthogonal polarization of the electric field (P=90). c) bianisotropic structure excited with polarization of the electric field along the grating lines (P=0). b) and d) the control structure with metal grating only for electrical-field polarizations P=90, and P=0, respectively. The vertical dashed lines indicates the spectral positions of the resonant peaks.

light. The difference in the resonance position partly arises because of the difference in the width of the grating lines, *but* is mostly due to the addition of the thin conducting layer, which alters the physical response of the system. Also note that the coupling to the plasmon can increase both the reflectance and absorption (not shown here),), hence the peak in reflection at the plasmonic resonance in figure 3; energy conservation then demands a reduction in transmission at the resonance, as observed in Figure 4.

When probing the metal grating with the electrical field polarized *along* the grating lines, (Figure 3b and d), both the plasmon resonance and the asymmetric reflection diminishes, and we are left with a reflection curve akin to that of a planar Au layer. Unlike the reflection spectra, the transmission curve (Figure 4) is independent of the illumination direction,

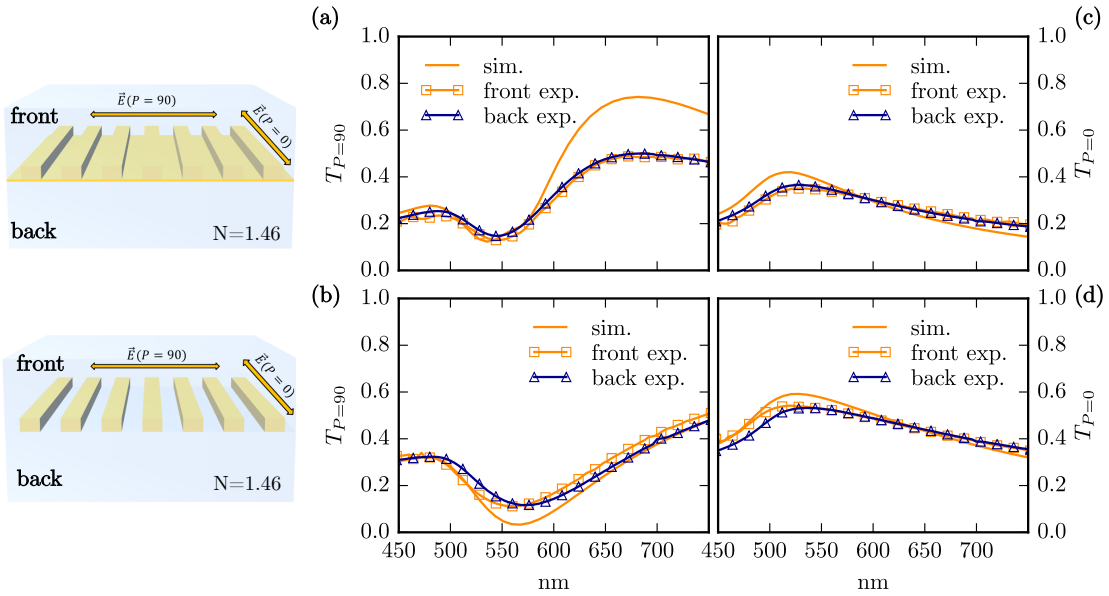

Figure 4: Transmission spectra. Open triangles and squares are the experimental results for 'back' and 'front' exposure, as defined in the illustration on the left to the plots; blue dashed and orange solid lines correspond to numerical simulations of 'back' and 'front' exposures. a) bianisotropic structure probed with orthogonal polarization of the electric field (P=90 in Figure 2). c) bianisotropic structure excited with polarization of the electric field along the grating lines (P=0 in Figure 2). b) and d) reflection spectra of the control structure with metal grating only for electrical field polarizations P=90, and P=0, respectively.

regardless to structure and polarization, as it must be due to reciprocity. For all structures and polarizations we see a qualitative agreement between experimental and numerical results with quantitative differences arising most likely from fabrication imperfections and uncertainties in the value of the permittivity.

It appears that an asymmetric reflection from our low profile structures is evident when the following two conditions are satisfied simultaneously: a) the device has to bear some optical asymmetry, and b) the incoming light has to be strongly coupled to, and absorbed by the active part of the device – here, achieved by means of plasmonic coupling between the incident light and the grating, when probed with the appropriate polarization. It is worth noting that, in *bulk* materials and structures, an optical asymmetry – and therefore asymmetric reflection – is abundant in nature and our daily life. Take for example a single side polished Silicon wafer, or a common bathroom mirror; both meet the former condition

above and demonstrate asymmetric reflection with one side reflecting more than the other. However, while the asymmetric reflection in the case of the two macroscopic examples given above is due to their two dissimilar non-interacting surfaces, achieving asymmetric reflection while maintaining a low structure profile at the order of $\lambda/10$, as demonstrated here, requires a design which meets also the second condition of strong coupling between the incoming light and the optically interacting surfaces.

As asymmetric reflection could only be observed for the grating with the 10nm connecting layer of gold, it is clear that understanding the role of the thin conducting layer is crucial for the understanding of the origin of the asymmetric reflection: the conductive layer electrically connects neighboring grating lines, therefore enabling a flow of electrical current in the direction normal to the grating lines (P=90). The induced current, in turn, generates a magnetic field[33] radiating energy into the far field and interfering with the incident wave. This effect is enhanced via a plasmon resonance, as more energy is coupled into the grating. However, the structural asymmetry leads to different coupling strengths for front or back illumination. If the light is incident on the flat side, the surface does not immediately provide the missing momentum to couple to plasmons so that a large fraction of the light is reflected. On the corrugated side, the surface immediately provides the missing momentum and coupling into plasmons is more efficient leading to higher absorption and thus reduced reflection properties. This behavior is well known from bianisotropic bulk materials exhibiting magneto-electric coupling.[19,23] In order to further investigate the magneto-electric coupling and quantify its strength, we continue by modeling our meta-surface as a bianisotropic metamaterial.[19,23]

Effective material parameters and bianisotropy

An asymmetric reflection/absorption spectrum cannot be described by a *homogeneous* slab model using effective permittivity and permeability alone; instead, magneto-electric coupling has to be introduced to the physical model by modifying the constitutive relations.[19,21,23] The magneto-electric coupling is quantified by new material parameters, $\boldsymbol{\zeta}$ and $\boldsymbol{\xi}$ (see intro-

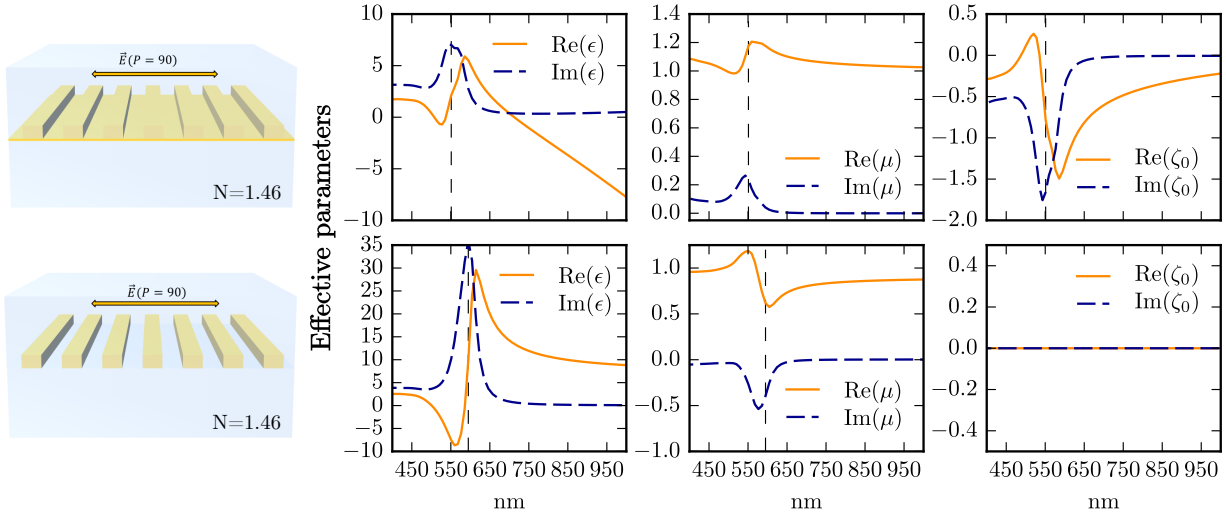

Figure 5: Effective material parameters retrieved from numerical simulations of the gold gratings described in figure 1. Results are for $P = 90$. The left column shows the effective permittivity, the middle column the effective permeability and the right column the bianisotropic coupling parameter. We used standard retrieval methods[21,23,34] and assumed a symmetric metamaterial slab with thickness d_{eff} equal to the maximum thickness of the gold gratings, i.e. $d_{eff} = 55$nm for the connected (top) and $d_{eff} = 45nm$ for the unconnected grating (bottom). The vertical dashed lines indicate the positions of the respective reflection maxima.

duction and section), which make the electric and magnetic fields interact in a way such that even a symmetric slab exhibits asymmetric reflection.[19,21,23]

We model our connected grating as a homogeneous bianisotropic slab and compare against the control grating. Note that the magneto-electric coupling parameters $\boldsymbol{\xi}$ and $\boldsymbol{\zeta}$ are determined by a single parameter ζ_0, on which we focus hereafter. For a determination of the effective material parameters, both the phase and magnitude of the reflection/transmission coefficient are needed. Since our experimental setup gives access to the magnitude, but not the phase, we subsequently focus on the simulations. Figure 5 shows the material parameters retrieved from simulations of the types of gold gratings structures for $P = 90$. Clearly, the interplay of plasmon resonance and structural asymmetry in the connected gold grating lead to an induced magneto-electric effect, as demonstrated by the strong resonance in the

coupling parameter ζ_0. The control grating, however, shows no such coupling, highlighting the importance of that thin connecting Au layer for the design. Figure 5 exhibits two additional differences between the bianisotropic and control gratings. First, though both samples feature optical magnetic effects (resonant permeability) at the plasmon resonance, the permeability of the control grating does not return to unity in the long wavelength limit, but remains weakly diamagnetic. This seemingly counter-intuitive result is explained as follows. In the long wavelength limit, gold approaches a perfect conductor, thus expelling part of the magnetic field from its interior. This results in 'squeezing' of the magnetic field lines through the gaps of the grating, leading to the diamagnetic effect observed.[35]The smaller the gap, the stronger this effect (see figure S3 in the Supporting Information).

The case of the bi-anisotropic sample with the connected grating is understood by analogy with a superconductor where the permeability is unity, but the permittivity diverges inversely as the frequency squared. In this case magnetic fields are expelled entirely through the action of the permittivity, contrary to some misinformed statements to the effect that superconductors are perfect diamagnets. In figure 5 top left we see that for the continuously connected sample the effective permittivity diverges at long wavelengths.

For the other polarization, $P = 0$, none of the effects above feature, as the electric field is polarized along the grating lines and current can flow freely in both the control and bi-anisotropic gratings, similar to the current flow in thin gold films. The effective material parameters for this case are shown in the Supporting Information (figure S4) for completeness.

Conclusion

We demonstrated experimentally and through simulations that plasmonic gratings provide a simple design for asymmetric reflectors/absorbers at visible wavelengths. We found that the asymmetry in the spectra is a direct consequence of magneto-electric coupling in the

grating, i.e. bianisotropy, and should be interpreted as such. The strength of the bianisotropy provides a good measure for the expected asymmetry in the spectra and may be used for the optimization of this effect, as has been done at much lower frequencies previously.[25] Finally, the bianisotropy of our grating is inherent to it, rather than induced by a substrate,[32] which leads to an extremely small footprint of the structure ($\approx 55nm$ thickness). Further optimizations in the grating design and fabrication are certain to enhance the strength of the asymmetry.

Methods

Experimental setup and fabrication

Fabrication of gratings structures: First, quartz substrates were cleaned by ultrasonic agitation in an acetone bath, followed up by IPA and DIW rinse. A Polymethyl methacrylate (PMMA 950, A4) positive resist spun on the cleaned substrates at 3500RPM for 60 seconds, and soft-baked on a hotplate at 180 C for 60 seconds, forming a 250 nm lift-off mask. Multiple arrays of grating lines were defined using a Raith eline Electron Beam Lithography tool at 10 kV accelerating voltage and 10 micro-meter aperture, and developed for 30 seconds in 1:3 methyl isobutyl ketone:isopropyl alcohol (MIBK:IPA) developer. Prior to the deposition of gold grating lines, the surface was modified to improve the adhesion of gold to the SiO2 substrate: a drop of (3-aminopropyl)triethoxysilane diluted in ethanol at a volumetric ratio of 1:25 was dropped and was left on the sample for 30 seconds before washed in ethanol and dried on a hotplate at 90C for 15 minutes. 45 nm of Au were thermally evaporated (Angstrom AMOD) at a rate of 2A/s. The fabrication of the grating pattern was completed by lift-off of the gold layer in acetone bath for 24H at room-temperature. After lift-off, the surface was functionalized again (as discussed above), and an additional layer of 10nm of Au was deposited on the sample (at a higher deposition rate of 5A/s to improve surface uniformity) through a mechanical mask that shaded half of the sample, completing the

control, and bianisotropic structures on a single substrate. The device was finished by bonding an additional quartz substrate on top, using a UV cured, indexed matched, low viscosity optical glue (Norland Optical Adhesive 85).

Reflection transmission measurements were carried out using a custom-made microscope set-up: The output of a Halogen lamp connected to a Bentham Instruments monochromator was coupled to a multimode optical fibre with a reflective collimator at its end. The collimated beam passed through a Glan-Thompson polarizer (Thorlabs) and a non-polarizing beamsplitter cube (coated with anti reflective-coating optimized to 400-700nm; Thorlabs) before entering a custom built microscope system and focused to a spot of diameter 50μm via 50X long-working distance objective lens with NA=0.5 (see Figure 2). The reflected and transmitted spectra were recorded using a Si photo-diode connected to a lock-in amplifier. Absolute transmission values were calculated by dividing the measured transmission photocurrent by the measured current without the sample. Absolute reflection values were calculated by first subtracting background reflections (originated mainly from the beam-splitter for wave-lengths below $\sim$450nm or above $\sim$680nm; measured for the same optical path without the sample) from the reflection photo-current, and from the reflectance measured from a calibrated silver coated mirror, and then dividing the back-ground-free reflectance current of the sample by that of the calibrated mirror.

Numerical modeling

The numerical simulations were carried out using the frequency domain solver of the commercial software package COMSOL Multiphysics (version 4.3a). We used the port boundary conditions to set up the exciting plane wave and periodic boundary conditions for the other two boundaries. The length of the simulation domain has been set to 1500nm and convergence with respect to it had been ensured. We used an adaptive triangular mesh with maximum element size of 2nm inside the gold gratings and 10nm in the surrounding medium; again convergence had been ensured. The exact dimensions of the gratings were chosen in

accordance with the experimental structures; detailed sketches can be found in the Supporting Information. We used experimental values for the permittivity of an evaporated gold film from.[36] The port boundary conditions allow to compute the scattering, i.e. S-parameters of the system, from which reflectance and transmittance can be deduced, as well as the effective material parameters.[21,23,34]

In this letter we modeled the two gratings as a bianisotropic metamaterial. That is, we replaced the whole system with a symmetric metamaterial slab of thickness d_{eff} and effective material parameters determined by the scattering parameters of the gratings. Bianisotropy means that the electric and magnetic fields inside such a material are coupled via[19,23]

$$\mathbf{D} = \boldsymbol{\epsilon}\mathbf{E} + \boldsymbol{\xi}\mathbf{H}$$

$$\mathbf{B} = \boldsymbol{\mu}\mathbf{H} + \boldsymbol{\zeta}\mathbf{E},$$

with permittivity and permeability tensor[19,23]

$$\boldsymbol{\epsilon} = \begin{pmatrix} \epsilon_x & 0 & 0 \\ 0 & \epsilon_y & 0 \\ 0 & 0 & \epsilon_z \end{pmatrix}, \boldsymbol{\mu} = \begin{pmatrix} \mu_x & 0 & 0 \\ 0 & \mu_y & 0 \\ 0 & 0 & \mu_z \end{pmatrix} \tag{1}$$

and magneto-electric coupling matrices[19,23] ,

$$\boldsymbol{\xi} = \begin{pmatrix} 0 & 0 & 0 \\ 0 & 0 & 0 \\ 0 & -i\xi_0 & 0 \end{pmatrix}, \boldsymbol{\zeta} = \begin{pmatrix} 0 & 0 & 0 \\ 0 & 0 & i\xi_0 \\ 0 & 0 & 0 \end{pmatrix}. \tag{2}$$

The magneto-electric coupling parameter that has been retrieved in this letter corresponds to the effective ζ_0. In our system we assumed the grating to lie in the y-z-plane, with the grating lines pointing along the z-direction and the periodic modulation along the y-direction. This means that for a wave traveling along the x-direction and polarized along

y (P=90 here), the effective permittivity and permeability component that are probed are ϵ_y and μ_z, respectively. Whereas the P=0 case probes ϵ_z and μ_y.

In our simulations we can access the S-parameters of the system by using 'Port boundary conditions'. However, the effective material parameters cannot be accessed directly in COMSOL. For this some post-processing is needed. Fortunately, standard methods have been developed to material parameters for a symmetric metamaterial slab from the S-parameters.[21,23,34] In our case, the thickness, d_{eff}, of this metamaterial slab was chosen to be the maximum thickness of the gold gratings.

Acknowledgement

The authors gratefully acknowledge support from the EPSRC EP/L024926/1 programme grant and the Leverhulme Trust. M.K. acknowledges support from the Imperial College PhD scholarship. A. B. acknowledges support from the Imperial College London Junior research fellowship. Y.L. acknowledges NTU-A*start Silicon Technologies of Excellence under the program grant No. 11235150003. S.A.M acknowledges the Royal Society and the Lee-Lucas Chair in Physics. J.B.P thanks the Gordon and Betty Moore foundation.

Supporting Information Available

Supporting Information is provided with this manuscript. The file contains detailed profiles of the gratings used in the simulations, a figure showing the mode profile at the plasmon resonance, a figure for the effective parameters for $P = 0$ polarization and a figure comparing the retrieved effective permeability for control gratings with different gap sizes between the grating lines. There are also enlarged SEM images of the bianisotropic and control grating. This material is available free of charge via the Internet at `http://pubs.acs.org/`.

References

(1) Landau, L. D.; Pitaevskii, L. P.; Lifshitz, E. M. *Electrodynamics of Continuous Media, Second Edition: Volume 8 (Course of Theoretical Physics)*, 2nd ed.; Butterworth-Heinemann, 1984.

(2) Shalaev, V. M. Optical negative-index metamaterials. *Nat. Photonics* **2007**, *1*, 41–48.

(3) Pakizeh, T.; Dmitriev, A.; Abrishamian, M. S.; Granpayeh, N.; Käll, M. Structural asymmetry and induced optical magnetism in plasmonic nanosandwiches. *J. Opt. Soc. Am. B* **2008**, *25*, 659–667.

(4) Ponsinet, V.; Barois, P.; Gali, S. M.; Richetti, P.; Salmon, J. B.; Vallecchi, A.; Albani, M.; Beulze, A. L.; Gomez-Grana, S.; Duguet, E.; Mornet, S.; Treguer-Delapierre, M. Resonant isotropic optical magnetism of plasmonic nanoclusters in visible light. *Phys. Rev. B* **2015**, *92*.

(5) Pendry, J.; Holden, A.; Stewart, W.; Youngs, I. Extremely low frequency plasmons in metallic mesostructures. *Phys. Rev. Lett.* **1996**, *76*, 4773–4776.

(6) Pendry, J. B.; Holden, A. J.; Robbins, D. J.; Stewart, W. J. Magnetism from Conductors and Enhanced Nonlinear Phenomena. *IEEE Trans. Microwave Theory Tech.* **1999**, *47*, 2075–2084.

(7) Smith, D. R.; Padilla, W. J.; Vier, D. C.; Nemat-Nasser, S. C.; Schultz, S. *Phys. Rev. Lett.* **2000**, *84*, 1–4.

(8) Merlin, R. Metamaterials and the Landau Lifshitz permeability argument : Large permittivity begets high-frequency magnetism. *Proc. Natl. Acad. Sci. U. S. A.* **2009**, *106*, 1693–1698.

(9) Holloway, C. L.; Kuester, E. F.; Gordon, J. A.; Hara, J. O.; Booth, J.; Smith, D. R.

An Overview of the Theory and Applications of Metasurfaces : The Two-Dimensional Equivalents of Metamaterials. *IEEE Trans. Antennas Propag.* **2012**, *54*, 10–35.

(10) Kildishev, A. V.; Boltasseva, A.; Shalaev, V. M. Planar Photonics with Metasurfaces. *Science* **2013**, *339*.

(11) Shi, J.; Fang, X.; Rogers, E. T. F.; Plum, E.; Macdonald, K. F.; Zheludev, N. I. Coherent control of Snell's law at metasurfaces. *Opt. Express* **2014**, *22*, 829–834.

(12) Meinzer, N.; Barnes, W. L.; Hooper, I. R. Plasmonic meta-atoms and metasurfaces. *Nat. Photonics* **2014**, *8*, 889–898.

(13) Stauber, T.; Gómez-Santos, G.; de Abajo, F. J. G. Extraordinary Absorption of Decorated Undoped Graphene. *Phys. Rev. Lett.* **2014**, *112*, 077401.

(14) Genevet, P.; Capasso, F. Holographic optical metasurfaces : a review of current progress. *Rep. Prog. Phys.* **2015**, *18*.

(15) Silva, A.; Monticone, F.; Castaldi, G.; Galdi, V.; Alù, A.; Engheta, N. Performing Mathematical Operations with Metamaterials. *Science* **2014**, *343*, 160–164.

(16) Yu, N.; Capasso, F. Flat optics with designer metasurfaces. *Nat. Mater.* **2014**, *13*, 139–149.

(17) Atwater, H. A.; Polman, A. Plasmonics for improved photovoltaic devices. *Nat. Mater.* **2010**, *9*, 205–13.

(18) Wu, C.; Iii, B. N.; John, J.; Milder, A.; Zollars, B.; Savoy, S.; Shvets, G. Metamaterial-based integrated plasmonic absorber / emitter for solar thermo-photovoltaic systems. *J. Opt.* **2012**, *14*.

(19) Kong, J. A. *Electromagnetic Wave Theory*, 6th ed.; EMW Publishing: Cambridge, MA, 2005.

(20) Kildishev, A. V.; Borneman, J. D.; Ni, X.; Shalaev, V. M.; Drachev, V. P. Bianisotropic Effective Parameters of Optical Metamagnetics and Negative-Index Materials. *Proc. IEEE* **2011**, *99*, 1691.

(21) Kriegeler, C. E.; Rill, M. S.; Linden, S.; Wegener, M. Bianisotropic Photonic Metamaterials. *IEEE J. Sel. Top. Quantum Electron.* **2010**, *16*, 367–375.

(22) Medina, F.; Rafii-el idrissi, R.; Marque, R. Role of bianisotropy in negative permeability and left-handed metamaterials . *Phys. Rev. B* **2002**, *65*, 1–6.

(23) Li, Z.; Aydin, K.; Ozbay, E. Determination of the effective constitutive parameters of bianisotropic metamaterials from reflection and transmission coefficients. *Phys. Rev. E* **2009**, *79*, 026610.

(24) Ra'di, Y.; Asadchy, V. S.; Kosulnikov, S. U.; Omelyanovich, M. M.; Morits, D.; Osipov, A. V.; Simovski, C. R.; Tretyakov, S. A. Full Light Absorption in Single Arrays of Spherical Nanoparticles. *ACS Photonics* **2015**, *2*, 653–660.

(25) Yazdi, M.; Albooyeh, M.; Alaee, R.; Asadchy, V.; Komjani, N.; Rockstuhl, C.; Simovski, C. R.; Tretyakov, S. A Bianisotropic Metasurface With Resonant Asymmetric Absorption. *IEEE Trans. Antennas Propag.* **2015**, *63*, 3004–3015.

(26) Aydin, K.; Li, Z.; Hudlicka, M.; Tretyakov, S. A.; Ozbay, E. Transmission characteristics of bianisotropic metamaterials based on omega shaped metallic inclusions. *New J. Phys.* **2007**, *9*.

(27) Pfeiffer, C.; Grbic, A. Bianisotropic Metasurfaces for Optimal Polarization Control : Analysis and Synthesis. *Phys. Rev. Appl.* **2014**, *044011*, 1–11.

(28) Zhao, J.; Sun, L.; Zhu, B.; Feng, Y. One-way absorber for linearly polarized electromagnetic wave utilizing composite metamaterial. *Opt. Express* **2015**, *23*, 383–387.

(29) Zhao, Y.; Belkin, M. A.; Alù, A. Twisted optical metamaterials for planarized ultrathin broadband circular polarizers. *Nat. Commun.* **2012**, *3*.

(30) Ra'di, Y.; Asadchy, V. S.; Tretyakov, S. A. Total Absorption of Electromagnetic Waves in Ultimately Thin Layers. *IEEE Trans. Antennas Propag.* **2013**, *61*, 4606–4614.

(31) Pfeiffer, C.; Zhang, C.; Ray, V.; Guo, L. J.; Grbic, A. High Performance Bianisotropic Metasurfaces: Asymmetric Transmission of Light. *Phys. Rev. Lett.* **2014**, *113*, 023902.

(32) Butun, S.; Aydin, K. Asymmetric Light Absorption and Reflection in Freestanding Nanostructured Metallic Membranes. *ACS Photonics* **2015**, *2*, 1652–1657.

(33) Kraft, M.; Luo, Y.; Maier, S. A.; Pendry, J. B. Designing Plasmonic Gratings with Transformation Optics. *Phys. Rev. X* **2015**, *5*, 031029.

(34) Chen, X.; Wu, B.-i.; Kong, J. A.; Grzegorczyk, T. M. Retrieval of the effective constitutive parameters of bianisotropic metamaterials. *Phys. Rev. E* **2005**, *71*, 1–9.

(35) Wood, B.; Pendry, J. B. Metamaterials at zero frequency. *J. Phys.: Condens. Matter* **2007**, *19*.

(36) Olmon, R. L.; Slovick, B.; Johnson, T. W.; Shelton, D.; Oh, S.-H.; Boreman, G. D.; Raschke, M. B. Optical dielectric function of gold. *Phys. Rev. B* **2012**, *86*, 235147.